Volume 5 | Number 4 | April 2018 | Pages 803–1046

Environmental Science Nano

rsc.li/es-nano

ISSN 2051-8153

ROYAL SOCIETY OF CHEMISTRY

PAPER

Mohammed Baalousha *et al.*

Natural organic matter composition determines the molecular nature of silver nanomaterial-NOM corona

Environmental Science Nano

PAPER

Cite this: *Environ. Sci.: Nano*, 2018, 5, 868

Natural organic matter composition determines the molecular nature of silver nanomaterial-NOM corona†

Mohammed Baalousha, *[a] Kamelia Afshinnia[a] and Laodong Guo [b]

Received 5th January 2018,
Accepted 4th February 2018

DOI: 10.1039/c8en00018b

rsc.li/es-nano

Adsorption of natural organic matter (NOM) on nanomaterials (NMs) results in the formation of interfacial area between NMs and the surrounding environment (referred to as NOM-corona), giving rise to NMs' unique surface identity. This unique surface identity is determined by the ligands and their interactions with NM surfaces. Since the chemical structure and functionality is heterogeneous and polydisperse, the molecular composition of NOM-corona is the result of competitive adsorption of NOM molecules on the NM surface. Here, we investigate the molecular composition of NOM-corona formed from two different NOM samples (isolated from the Yukon River and Milwaukee River) on the surface of AgNMs using electrospray ionization-Fourier-transform ion cyclotron resonance mass spectrometry (ESI-FT-ICR-MS). The composition of AgNM-NOM corona varied with the composition of the original NOM. In general, AgNM-NOM corona is rich with N- and S-containing compounds. Furthermore, AgNM-NOM corona is rich with compounds with high molecular weight, high unsaturation, and high number of oxygenated groups. However, CHOS (carbon, hydrogen, oxygen and sulfur) compounds adsorbed on AgNMs from the Yukon River NOM have low molecular weight (LMW) and low saturation index, which might be due to selective adsorption *via* chemical complexation (Ag–S). On the other hand, NOM compounds with LMW and low unsaturation or compounds containing few oxygenated groups (mainly alcohols and ethers) are preferentially maintained in solution phase. The results here provide evidence of molecular interactions between NOM and NMs, which are critical to understanding NM behavior and toxicity in natural environments.

Environmental significance

Natural organic matter-corona (NOM-corona) is an interfacial area between nanomaterials (NMs) and the surrounding environment, which gives rise to NMs' unique surface identity. This study demonstrates that the composition and properties of AgNOM-corona depends on NOM molecular properties and is dominated by the selective sorption of N- and S-containing NOM molecules, highly unsaturated, and high molecular weight molecules. In addition, NOM compounds with low molecular weight and low unsaturation or compounds containing few oxygenated groups (mainly alcohols and ethers) are preferentially maintained in solution phase. The results here provide evidence of molecular interactions between NOM and NMs, which are critical to understanding NM behavior and toxicity in the natural environment.

1. Introduction

Natural organic matter (NOM) is ubiquitous in natural environments and varies in concentration from 0.1 to 10's of mg C L^{-1}, depending on biogeochemical and climatic conditions.[1,2] It has been long known that NOM interacts with metals,[3] organic pollutants[4] and surfaces of nanomaterials,[5] and NOM adsorption results in chemical fractionation between particle surfaces and solution.[6,7] Selective adsorption of NOM on nanomaterial (NM) surfaces results in formation of a surface coating (*i.e.*, NOM-corona),[8] giving NMs a unique surface identity. NOM-corona is the primary interface that determines NM surface characteristics (*e.g.*, reactivity, adsorption capacity, charge), environmental behavior (*e.g.*, aggregation,[9–11] dissolution,[12–14] and sulfidation[15]), and biological interactions (*e.g.*, bioavailability and toxicity),[16] and these processes are anticipated to depend on NOM composition and thus NOM-corona composition. Understanding NOM-corona characteristics is fundamental to understanding NM environmental and biological interactions.

NOM is a large pool of carbon-based compounds derived from chemical and biological degradation of plant and

[a] *Center for Environmental Nanoscience and Risk, Arnold School of Public Health, University South Carolina, Columbia, South Carolina 29208, USA. E-mail: mbaalous@mailbox.sc.edu*
[b] *School of Freshwater Sciences, University of Wisconsin-Milwaukee, 600 E Greenfield Ave., Milwaukee, WI 53204, USA*

† Electronic supplementary information (ESI) available. See DOI: 10.1039/c8en00018b

animal residues. NOM is composed of a complex mixture of polyelectrolytic and polyfunctional organic molecules (tens of thousands of unique chemical species) that vary spatially and temporally in molecular composition, acidity, molecular weight and structure, and charge density.[17] The polydispersity in composition and physical and chemical properties of NOM impacts the molecular composition of NOM-corona, and influences NM fate, behavior, bioavailability and toxicity. For instance, higher molecular weight NOM increases the stability of AuNMs due to increased electrosteric repulsion.[18–21] Additionally, aggregation of ZnS particles (laboratory simulation of natural ZnS particles) decreased with increasing NOM concentration, molecular weight, and aromatic content of NOM fractions.[22] Some studies reported that Suwannee River humic acid (SRHA) and fulvic acid (SRFA) did not alter AgNMs dissolution,[12] but others reported suppression of AgNM dissolution by SRHA[13] and SRFA.[14] Similarly, one study reported that Pony Lake fulvic acid (PLFA) significantly decreased AgNM dissolution due to PLFA's sulfur and nitrogen content,[12] but others have reported that PLFA increased AgNM dissolution.[23] In addition, NOM has been shown to enhance the dissolution of other NMs such as ZnO (ref. 24) and Cu,[25] due to complexation of divalent cations (Zn^{2+}, Cu^{2+}) by NOM functional groups. These apparent contradictory results may be attributed to differences in the molecular composition of NOMs.

Similarly, the impact of NOM on NM bioavailability and toxicity is complex; *i.e.*, even for the same type of NMs, enhanced,[26] mitigated[27,28] and non-significant effects[29] have been observed. For instance, PLFA mitigated AgNM toxicity to the nematode *Caenorhabditis elegans* more effectively than SRFA,[30] which was attributed to the higher metal binding capacity of PLFA compared to SRFA due to compositional differences between these two NOMs. PLFA has higher N and S contents (6.5% N, 3.0% S) than SRFA (0.72% N, 0.44% S), suggesting that PLFA has a higher percentage of amine ligands and reduced sulfur groups that provide more binding sites for Ag^{+} and AgNM surfaces.[31,32] Tannic acid has also been shown to reduce ZnO toxicity more efficiently than FA and HA by reducing bioavailability of free Zn^{2+} in aqueous media.[33] This is because tannic acid has a higher affinity to Zn^{2+} among tested NOMs due to formation of stable tannic acid–Zn^{2+} complexes *via* highly concentrated O-diphenol groups on the tannic acid surface. In addition, compared to NOM samples, proteins and carbohydrates were less effective in mitigating ZnO-NMs toxicity in embryonic zebrafish.[16] However, the specific mechanisms are largely unknown. Therefore, acquiring a comprehensive description at the molecular level of the composition of NOM-corona on NM surfaces is sorely needed.

During the last two decades, there has been a growing interest in getting a detailed understanding of the behavior of NOM compounds during adsorption onto NMs interfaces. Spectroscopic evidence identifies strong sorptive fractionation that occurs between diverse organic compounds of humic substances.[7,34,35] In addition, the hydrophobic fraction of fulvic acids (and/or the organic molecules with high contents in aromatic moieties activated by oxygenated functionalities) were preferentially sorbed compared to aliphatic fractions on metallic oxide mineral surfaces.[7,34,36] Moreover, size-exclusion-chromatography and spectroscopic analysis of fulvic or humic acids highlight the fractionation of molecules based on size during adsorption to mineral surfaces,[37] which was attributed to structural trends in the molecular weight fractions (*e.g.*, degree of aromaticity, chemical functionality and the underlying adsorption processes). Selective adsorption of high molecular weight (HMW) compounds, aromatic,[38] hydrophobic compounds[38] has been reported on the surface of natural and engineered NMs through bulk measurement techniques (*i.e.*, fractionation and UV-vis). However, few studies describe the molecular level composition and properties of NOM molecules that selectively sorb on the surface of NMs. Moreover, most previous studies used humic substances extracted by a highly operationally defined chemical procedure, such as PLFA, SRFA and SRHA provided by the International Humic Substances Society. Although humic substances are a major NOM component in aquatic environments, NOMs also contain other organic compounds that may not be isolated using solid phase extraction methods used to isolate humic and fulvic acids. Thus, NOMs extracted by physical separation, such as ultrafiltration methods, likely contain a broader spectrum in NOM composition or functionalities.[39,40]

Recently, the development of an advanced technique, namely ultra-high resolution-Fourier transform-ion cyclotron resonance-mass spectrometry (FT-ICR-MS) offers resolving power sufficient for identification of NOM compounds at the level of elemental composition assignment. FT-ICR-MS is a technique that measures the mass-to-charge ratio of organic compounds with up to six decimal place precision.[41] Thus, FT-ICR-MS provides elemental composition assignment for compounds with the same nominal mass-to-charge ratio (m/z), but differing in exact mass, critical to elucidate NOM and selective adsorption to NMs. Few studies have addressed the molecular-level characterization of NOM formulas that selectively sorb on the surface of minerals using ultrahigh resolution FT-ICR-MS. For instance, enrichment of highly reactive, acidic, oxygen functionalized aromatic and aliphatic molecules has been reported, and of highly condensed aromatic compounds depleted in hydrogen carrying only a few oxygenated groups were selectively sorbed on alumina surfaces.[42,43] Another study demonstrated that Ferrihydrite exhibited higher affinity to NOM than did goethite or lepidocrocite, and HMW (>500 Da) compounds and compounds high in unsaturation or rich in oxygen (including polycyclic aromatics, polyphenols and carboxylic compounds) had higher affinity to iron oxyhydroxides, and especially ferrihydrite.

Here, we characterize NOM-corona formed on the surface of citrate-coated silver nanomaterials (cit-AgNMs) at the molecular level through negative-ion electrospray ionization FT-ICR-MS. Comparisons of molecular signatures derived from two HMW-NOM samples isolated from the Yukon River and

the Milwaukee River by ultrafiltration that form NOM-corona provide new insights into NOM–NM interactions.

2. Materials and methods

2.1. Synthesis and characterization of nanomaterials

Citrate-coated silver nanomaterials (cit-AgNMs) were synthesized as reported in previous studies.[31] Briefly, a 100 mL of 0.31 mM trisodium citrate, 100 mL of 0.25 mM silver nitrate, and 10 mM of sodium borohydride solutions were prepared in ultra-pure water and kept at 4 °C in the dark for 30 min. The silver nitrate and trisodium citrate solutions were combined together, vigorously stirred, and then 6 mL of sodium borohydride ($NaBH_4$), a reducing agent, was added. The solution was stirred for 10 min, heated slowly to boiling, boiled for 90 min, and cooled to 4 °C in the dark. AgNMs were then cleaned, to remove the excess reagents before use, by ultrafiltration (Amicon, 1 kDa regenerated cellulose membrane, Millipore) using a diafiltration method to prevent NM aggregation and drying. AgNMs were re-dispersed in 0.31 mM trisodium citrate solution to avoid further growth; this process was repeated a minimum of three times. The concentration of AgNMs was measured by inductively coupled plasma-optical emission spectrometry (ICP-OES) and was about 7.72 ± 0.001 mg-Ag L^{-1}.

2.2. Solution chemistry

Two HMW-NOM (1 kDa–0.45 μm) samples, isolated from the Yukon River (YRNOM), Alaska, and the Milwaukee River (MRNOM), Wisconsin, USA by ultrafiltration,[44] were compared to highlight compositional differences between NOM-corona formed by selective adsorption of NOM molecules on the surface of cit-AgNMs. Stock solutions of NOM samples (100 mg L^{-1}) were prepared by dissolving 2 mg of freeze dried NOM in 20 mL ultrapure water. The pH was adjusted to 7.0 through addition of 0.1 or 1 M NaOH. Each suspension was filtered through a 100 nm filter to remove any aggregated molecules. Total organic carbon (TOC) and specific UV absorbance ($SUVA_{254}$) was calculated as the ratio of UV-vis absorbance at λ_{254} to TOC concentration.[45] $SUVA_{254}$ was 3.24 and 3.91 L mg^{-1} m for the YRNOM and MRNOM sample, respectively.

Aliquots of cit-AgNM stock suspension was diluted in ultrapure water (18.2 MΩ cm) and mixed with predetermined amounts of NOM and sodium bicarbonate buffer to yield a final AgNM concentration of 4 mg-Ag L^{-1}, and all measurements performed with 5 mg L^{-1} of NOM and 0.1 mM sodium bicarbonate buffer addition to maintain a constant pH at 8.2–8.4 and constant ionic strength at 0.1 mM for the experimental duration. Mixed NM and NOM suspensions were left for 24 hours to equilibrate. NMs and NOM suspension mixture was then ultrafiltered (using an Amicon stirred cell unit, with 10 kDa regenerated cellulose ultrafiltration disc, Millipore YM-10) to separate NMs from the <10 kDa ultrafiltrate. Similarly, control samples that contained NOM and no NMs were ultrafiltered on 10 kDa membranes. Filtrates were collected in amber HDPE bottles and shipped overnight to the National High Magnetic Field Laboratory Ion Cyclotron Resonance facility at Florida State University (Tallahassee, Florida) for electrospray ionization FT-ICR mass spectral analysis.

2.3. Characterization of NOM-corona

FT-ICR-MS. NOM samples were analyzed using a custom build 21 T FT-ICR-MS[46] to monitor compositional changes that occur in NOM before and after selective adsorption by cit-AgNMs. NOM samples were acidified to pH 2 with HCl extracted by solid-phase extraction (SPE) on PPL (modified styrene divinyl benzene polymer type sorbents) cartridges, and eluted with HPLC-grade methanol to concentrate NOM and remove salts.[47,48] NOM samples were analyzed using a 21 T FT-ICR-MS using microelectrospray ionization in negative mode. For each spectrum, 100 scans ($200 < m/z < 1200$) were co-added, apodized with a full Hanning weight function, and zero-filled once prior to fast Fourier transformation.[2] ICR frequencies were converted to ion masses based on the quadrupolar trapping potential approximation.[49] Each spectrum was scaled according to the most abundant peak, internally calibrated based on the "walking" calibration equation[50] for a highly abundant homologous series (mass of $-CH_2-$ repeating unit 14.01565 Da) confirmed with isotopic fine structure.

Elemental compositions assignment was facilitated by PetroOrg© software[3] and further detailed in ESI.† The following criteria were used for assignment of molecular formulas to the peaks detected on the mass spectra: signal-to-noise ratio of peak (S/N) ≥ 6; mass accuracy better than 0.5 ppm; elemental constraints O ≤ 25, C ≤ 100, H ≤ 200, N ≤ 3, and S ≤ 2. Molecular weight (MW), hydrogen to carbon ratio (H/C), oxygen to carbon ratio (O/C), oxygen to sulfur ratio (O/S), oxygen to nitrogen ratio (O/N), double bond equivalent (DBE, number of rings plus double bonds to carbon),[4] and modified aromaticity index (AI_{mod}, eqn (1))[51] were calculated from each elemental formulas. Elemental ratios (H, C, O/C, and O/S) were calculated by dividing the number the corresponding atoms in each assigned formula.

AI_{mod}. AI_{mod} and DBE estimate the degree of aromaticity for organic compounds calculated from elemental composition.[51] A low AI_{mod} indicates a low degree of aromaticity, where a value of zero is an aliphatic compound, a value between 0 and 0.5 is representative of olefinic compounds (containing at least one double bond) and includes alicyclic molecules.[52] A high AI_{mod} indicates a higher degree of aromaticity where a compound having a value of 0.5 is aromatic, and a value ≥0.67 indicates condensed aromatic compounds (fused rings).[38,51] Aromaticity index has been widely used to evaluate the aromaticity of a given molecular formula. By using AI_{mod} and element ratios of H/C, all the detected molecules displayed in the van Krevelen diagram were divided into four groups according to their molecular components (Table S1†). Molecules with Mod $AI_{mod} \geq 0.67$ are classified as condensed

aromatics, $0.5 <$ Mod $AI_{mod} < 0.67$ are classified as aromatics, and molecules with Mod $AI_{mod} \leq 0.5$ thus have an aliphatic character that is more or less pronounced (aliphatic compound or compound carrying many and/or long aliphatic chains).[38,43]

$$AI_{mod} = \frac{1 + C - 0.5\,O - 0.5\,H - S - N}{C - 0.5\,O - S - N} \quad (1)$$

Double bond equivalents. DBE indicates the number of double bonds and/or rings to carbon and is calculated according to eqn (2).[53]

$$DBE = c - \frac{H}{2} + \frac{N}{2} + 1 \quad (2)$$

NOM-corona composition. For NOM-corona composition, only elemental compositions selectively removed to AgNM surfaces following NOM adsorption were considered, as these represent the compounds with the highest affinity to AgNM surface. However, because FT-ICR-MS provides accurate mass measurements that correspond to elemental compositions, structural isomers are not differentiated. The selectively sorbed NOM molecules corresponded to elemental compositions present in NOM prior to AgNMs adsorption, but absent in NOM after adsorption to AgNMs identified with PetroOrg.

3. Results and discussion

NOM-corona formation on surfaces and NMs has been demonstrated by measuring coating thickness on mica sheets by atomic force microscopy,[5] iron oxides NMs by field flow fractionation,[54,55] or thickness of oxygen rich layer around AgNMs with transmission electron microscopy-coupled with electron energy loss spectrometry.[56] Suwannee River humic acid (SRHA) has been shown to form a 1–3 nm thick surface coating on freshly cleaved mica surface, and the thickness of this coating increased with decreasing pH and increasing exposure time.[5] Similarly, SRHA has been shown to form a <1 nm thick surface layer around 7 nm iron oxide NMs, and the thickness of this layer increased with the increase in SRHA concentration.[54,55] Suwannee River fulvic acid (SRFA) has been shown to form a 1.3 nm oxygen-containing corona around 20 nm citrate coated AgNMs.[56] However, little is known about the elemental composition and molecular properties of NOM molecules that form NOM-corona. Only FT-ICR-MS achieves resolving power and mass accuracy sufficient to identify NOM compounds at the molecular level.[38] Here, NOM-corona is the ensemble of molecules selectively sequestered (removed from solution) on AgNM surfaces. NOM-corona composition was determined as the difference between elemental compositions (as mass-to-charge ratios, m/z) present in original NOM but absent from ultrafiltered NOM after interaction with AgNM surfaces. However, this method only delineates between m/z ratios unique to each sample, but does not account for isomeric separation.

3.1. Mass spectra of NOM and corresponding AgNM-NOM corona

Fig. S1a and S2a† shows the broadband negative-ion ESI FT-ICR-MS mass spectra for all mass spectral peaks above six-times-the baseline RMS noise level detected in original YRNOM and MRNOM that highlight NOM compositional complexity.[38] The FT-ICR-MS spectra of the YRNOM and the MRNOM reveal a tri-modal distribution of peaks with the first between m/z 200 and 350, the second between m/z 350 and 600, and the third between m/z 600 and 1000. Based on the occurrence of carbon isotope peak twins with a distance of 1.0034 m/z, nearly all ions were singly charged[57] as previously reported.[58] The molecular weight distribution determined by FT-ICR-MS is <1 kDa, in agreement with previous reports of the supramolecular assembly concept.[59] Each FT-ICR spectrum was optimized based on a low resolution linear ion trap prescreen. Mass spectra of YR and MR AgNM-NOM corona are dominated by spectral peaks with $m/z > 400$ (Fig. S3a and 4a†), indicating selective adsorption of NOM formulas with higher molecular mass, consistent with previous reports.[18]

3.2. NOM-corona composition

Heteroatom classes of compounds. More than 13 000 mass spectral peaks with signal magnitude $>6\sigma$ for YRNOM and MRNOM were assigned elemental compositions, with RMS error <500 ppb across the entire distribution. The assigned compounds correspond to four compound types: carbon, hydrogen, and oxygen (CHO); carbon, hydrogen, oxygen, and nitrogen-containing (CHON); carbon, hydrogen, oxygen, and sulfur containing (CHOS); and compounds that contain carbon, hydrogen, oxygen, nitrogen and sulfur (CHONS). The YRNOM contained only CHO, CHON, and CHOS compounds; whereas, the MRNOM contained CHO, CHON, CHOS, and CHONS compounds. CHONS formulas in MRNOM are likely to be protein-like material (*e.g.*, amino acids), in good agreement with the excitation emission spectra of MRNOM (Fig. S5b, Table S2†). In the YRNOM, 6603 (50.6% formulas, 85.6% relative abundance, (RA)) of the compounds were CHO, 5235 (40.1% formulas, 12.2% RA) of the compounds were CHON, 1214 (9.3% formulas, 2.2% RA) of the compounds were CHOS, and 0 (0%) of the compounds were CHONS (Table 1). In the MRNOM, 5425 (40.7% formulas, 66.9% RA) of the compounds were CHO, 5893 (44.2% formulas, 26% RA) of the compounds were CHON, 1518 (11.4% formulas, 5.8% RA) of the compounds were CHOS, and 501 (3.8% formulas, 1.3% RA) of the compounds were CHONS (Table 1). The differences are likely due to differences in sources/processing of the NOM samples, rather than due to ionization and detection variations in the measurement technique as all samples were separated, extracted, and analyzed using the same protocol and at the same time.

Table 1 Properties of NOM and AgNM-NOM corona. Experiments were performed at 4 mg L^{-1} cit-AgNP and 5 mg L^{-1} NOM concentrations

	Formulas	# of assigned formulas	Formulas % in NOM-corona	Formulas % in original NOM	RA %	AMW	DBE	H/C	O/C	AI_{mod}
YR NOM	All	13 052	100	—	100	**560.1**	**14.0**	1.11	0.58	0.34
	CHO	6603	50.6	—	85.6	**557.6**	**14.0**	1.11	0.58	0.34
	CHOS	1214	9.3	—	2.2	**556.6**	**9.70**	1.36	0.48	0.15
	CHON	5235	40.1	—	12.2	**574.9**	**14.8**	1.08	0.59	0.34
	CHONS	—	—	—	—	—	—	—	—	—
MR NOM	All	13 337	100	—	100	**597.4**	**15.5**	1.02	0.59	0.37
	CHO	5425	40.7	—	66.9	**594.1**	**15.2**	1.03	0.59	0.37
	CHOS	1518	11.4	—	5.8	**571.1**	**13.6**	1.08	0.63	0.29
	CHON	5893	44.2	—	26.0	**613.2**	**16.50**	0.97	0.58	0.39
	CHONS	501	3.8	—	1.3	**549.8**	**14.7**	0.90	0.61	0.40
Cit-AgNMs										
YR-NOM corona	All	2398		18.4	100	**742.7**	**17.6**	1.19	0.52	0.30
	CHO	549	22.9	8.3	24.8	**823.6**	**19.1**	1.20	0.55	0.31
	CHOS	647	27.0	53.3	31.5	**641.9**	**10.9**	1.40	0.40	0.16
	CHON	1202	50.1	23.0	43.6	**775.1**	**19.5**	0.97	0.59	0.39
	CHONS	—		—	—	—	—	—	—	—
MR-NOM corona	All	1815	100	13.6	100	**776.2**	**20.2**	0.96	0.59	0.40
	CHO	432	23.8	8.0	26.7	**829.0**	**20.4**	1.05	0.54	0.38
	CHOS	300	16.5	19.8	17.1	**705.3**	**17.3**	0.98	0.66	0.34
	CHON	988	54.4	16.8	51.4	**780.0**	**21.0**	0.90	0.59	0.42
	CHONS	95	5.2	19.0	4.9	**634.9**	**17.1**	0.86	0.62	0.42

For the AgNM-NOM corona formed by adsorption of YRNOM, 2398 formulas were assigned to AgNM-NOM corona, representing 18.4% of all formulas in the YRNOM. Among the formulas forming AgNM-NOM corona, 549 (22.9% formulas and 24.8% RA), 647 (27% formulas and 31.5% RA), and 1202 (50.1% formulas and 43.6% RA) were CHO, CHOS and CHON, respectively, indicating that the majority (77% of all AgNM-NOM corona formulas and 75.1% of the total relative abundance of all assigned formula) of NOM formulas in AgNM-NOM corona are CHON followed by CHOS (Table 1). CHO, CHOS and CHON formulas in AgNM-NOM corona represented 8.3%, 53.3% and 23.0% of total number of respective assigned formulas in the raw NOM, indicating selective adsorption of CHOS and CHON formulas compared with CHO formulas.

Similarly, for the AgNM-NOM corona formed by adsorption from MRNOM, 1815 formulas were assigned to AgNM-NOM corona, representing 13.6% of formulas in MRNOM. Among the formulas forming AgNM-NOM corona, 432 (23.8% formulas and 26.7% RA), 300 (16.5% formulas and 17.1% RA), 988 (54.4% formulas and 51.4% RA), and 95 (5.2% formulas and 4.9% RA) were CHO, CHOS, CHON, and CHONS respectively (Table 1), indicating that the% number and% relative abundance of formulas in AgNM-NOM corona follow the trend CHON > CHO > CHOS > CHONS. The majority (76.2% of all AgNM-NOM corona formulas and 73.3% of the total relative abundance of all assigned formula) of NOM formulas in AgNM-NOM corona contain S and N heteroatoms. CHO, CHOS, CHON and CHONS formulas in AgNM-NOM corona represented 8.0%, 19.8%, 16.8%, and 19.0% of total respective assigned formulas in the raw NOM, indicating selective adsorption of CHOS and CHON and CHONS compared with CHO formulas.

These results clearly indicate that S- and N-containing compounds/functionalities play a major role in determining the molecular make-up of AgNM-NOM corona, despite their low abundance (S = 0.5% to 3.0%,[60,61] and N = 0.5–5% by weight[62]) in NOM.[63] This is in agreement with the study by Gunsolus *et al.* suggesting that S and N content (*i.e.*, sites with high affinity for metallic silver and Ag^{+}) plays a significant role in determining NOM interaction with AgNMs in addition to molecular weight.[12] NOM contains several functional groups that can bind silver such as –COOH, –OH, $–NR_2$, and $–SR_2$ with R as $–CH_2–$ or –H.[64] Thiol and amine groups are mainly responsible for Ag complexation while oxygen-containing functional groups have only minor effects on Ag binding to NOM.[65,66] This is also consistent with stability constants of S-, N-, and O-containing functional groups. The values for $\log K$ for silver complexes follow the order inorganic sulfide (14–21) > organic sulfide (12–15) > N (NH_3 and amines, 3–6) > Cl^- (3) > O (carboxyl and hydroxyl groups < 2).[66–70] Thus, in general, reduced sulfur ligands will react first with AgNMs followed by N-ligands and finally O-ligands.[71]

Sulfur in NOM occurs as reduced (*e.g.*, sulfide, thiol) or as oxidized species (*e.g.*, sulfonate, sulfate), with oxidation state ranging from −2 to +6. Of these, only reduced sulfur sites are expected to be important for Ag binding. However, reduced sulfur from aquatic environments can account for 20–70% of total sulfur as a combination of highly reduced exocyclic S (*e.g.*, thioethers (R-S-R), cyclic thioethers, and thiolate (R-S-/S-SH)) and moderately reduced heterocyclic species (*e.g.*, thiophene).[61,72–76] Exocyclic reduced sulfur represents 29 to 42%, heterocyclic reduced S represents 25–35%, while oxidized sulfur (*e.g.*, sulfoxide, sulfone, sulfonate, and organisulfate) represents 23–38% of total sulfur in aquatic NOM.[61,76] Heterocyclic reduced sulfur species (*e.g.*, thioethers as in methionine with $\log K = 3$) do not bind silver strongly[77] and disulfides (R-SS-R) do not form significant complexes

with Ag^+,[78,79] and only one silver-disulfide structure is known.[77] Thus, only a fraction – mainly exocyclic reduced sulfur containing compounds – of CHOS compounds are expected to contribute to the formation of AgNM-NOM corona.

Organic nitrogen incorporated into NOM accounts for more than 90% of the total nitrogen in soils,[80] sediments and aquatic environments. Its primary source is biochemical nitrogen from dead plant and animal residues (predominantly proteinaceous substances). N is typically present in aquatic dissolved organic matter in the form of amides, amines, and heterocyclic nitrogen.[81–83] Nitrogen-containing functional groups play important role in organic ligand–metal particle interactions. For instance, among DNA bases (*e.g.*, adenine, guanine, cytosine, and thymine), AgNMs interact strongest with cytosine due to its exocyclic nitrogen and weakest with thiamine due to the absence of an exocyclic amine.[84] Similarly, nitrogen sites in polyacrylamide act as partial electron acceptors from metallic nanoparticles and thereby create an attractive physical or weak chemical interaction leading to the adsorption of the metal particle specific to the nitrogen sites in the pendant of the polymer molecules.[85]

Additionally, S- and N-containing organic ligands have a range of affinities to Ag. For instance, mercaptants show very strong binding with $\log K$ values around 13, whereas doubly bonded sulfur and thioethers (*e.g.*, dimethyl sulfide, $\log K$ = 3.7) have $\log K$ values similar to those of amines (*e.g.*, methylamine, $\log K$ = 3.06).[77] The presence of multiple amine functions, as in tetraethylene pentamine, can considerably increase the value of $\log K$ (*e.g.*, $\log K$ = 7.4). On the other hand, carboxylates have very low $\log K$ and only with multifunctional species, such as EDTA, do values become significant. Thus, the co-occurrence of S- and N-ligands/formulas in AgNM-NOM corona.[77]

Comparing AgNM-NOM corona formed from the YRNOM and MRNOM indicates higher selectivity for adsorption of CHOS formulas from the YRNOM (*e.g.*, 53.3% of all formulas were selectively removed on the surface of AgNM, Table 1) compared to the MRNOM (*e.g.*, 19.8% of all formulas were selectively removed on the surface of AgNM, Table 1). The difference in the selectivity of CHOS formulas between the YRNOM and MRNOM can be attributed to the difference in their molecular characteristics. CHOS formulas in the YRNOM are characterized by higher relative abundance of aliphatic compounds (Table S3†), lower MW, DBE, O/C, and AI_{mod}, and higher H/C compared to those in the MRNOM (Table 1).

It is worth noting here that, the other compounds that did not selectively sorb on AgNMs displayed a lower intensity in the ultrafiltered samples (<10 kDa) after adsorption to AgNMs than in the corresponding original NOM. The magnitude of the decrease in intensity (from NOM before to after adsorption to AgNMs) varied considerably depending on specific compounds. This indicates that these compounds were partitioned between the solution and the surface of AgNMs to different extents, showing different affinities for the surface.

Biogeochemical classes of compounds. Elemental compositions derived from FT-ICR-MS spectra can be rapidly visualized in van Krevelen diagrams,[58] which plot H/C ratio *versus* O/C ratio. Every data point represents a single monoisotopic elemental composition derived from NOM, with color on the *z*-axis that indicates relative abundance. Compound classes (*e.g.*, aromatics, polyphenols and aliphatic) are located in different regions of the van Krevelen diagram as described in detail elsewhere.[58]

Fig. 1 shows van Krevelen diagrams for identified compounds in both NOMs. Fig. 1a and e suggest that the organic compounds in YRNOM correspond to species with slightly higher H/C (1.11) compared to MRNOM (1.02; Table 1), and that both NOMs have similar O/C ratios. CHO compounds (Fig. 1b and f) are the most abundant (85.6% and 66.9% RA for the YRNOM and MRNOM, respectively, Table 1) class detected by ESI FT-ICR-MS of NOM.[6,8–15] CHON formulas (Fig. 1c and g) in the YRNOM span wider O/C and H/C ranges compared with those in the MRNOM, with approximately identical relative-abundance weighted average O/C (0.58–0.59, Table 1) and higher H/C in the YRNOM (1.08) compared to MRNOM (0.97), which could indicate that YRNOM contains a slightly higher proportion of aliphatic compounds ($1.5 \leq$ H/C ≤ 2.0). The most noticeable differences are observed for the CHOS compounds (Fig. 1d and h). The YRNOM contained CHOS compounds with low O/C (0.2–0.4, Fig. 1d) together with CHOS formulas with high O/C (0.4–0.9, Fig. 1d) with an average value of 0.48 (Table 1); whereas, the MRNOM contained CHOS formulas with high O/C (0.4–0.9, Fig. 1h) with an average O/C of 0.63 (Table 1).

The van Krevelen diagram of all, CHO, CHON, CHOS and CHONS formulas forming AgNM-NOM corona formed by selective adsorption of NOM formulas from YRNOM and MRNOM are presented in Fig. 2. Results in Fig. 2a and b show an evident selective adsorption of compounds with relatively high O/C (*ca.* 0.5–1.0) and low H/C (*ca.* 0.5–1.2) ratios in both YRNOM and MRNOM, except for a group of compounds at low O/C and high H/C values in the YRNOM, which are sulfur rich compounds (Fig. 2d).

Based on their locations in the van Krevelen diagram, NOM formulas in YRNOM and MRNOM were assigned to different biogeochemical compound classes (Fig. 3, Table S3†). The relative distribution of the biogeochemical compound classes in all assigned formulas and in each heteroatom class of compounds is shown in Fig. 3a and b. The most abundant compounds correspond to highly unsaturated and phenolic compounds (HUPC, 75%) and polyphenolic compounds in both samples (YRNOM = 16% and MRNOM = 19%), typical of riverine NOM.[86] The proportion of condensed polycylic aromatics (CPA) and aliphatic compounds were 4.2 and 3.7% for the YRNOM and 3.9 and 1.0% for the MRNOM. CHO, CHON, and CHONS formulas generally follow the same trend as all assigned formulas. However, YRNOM CHOS compounds were mainly HUPC (75.3% RA) and aliphatic (22.4% RA), with

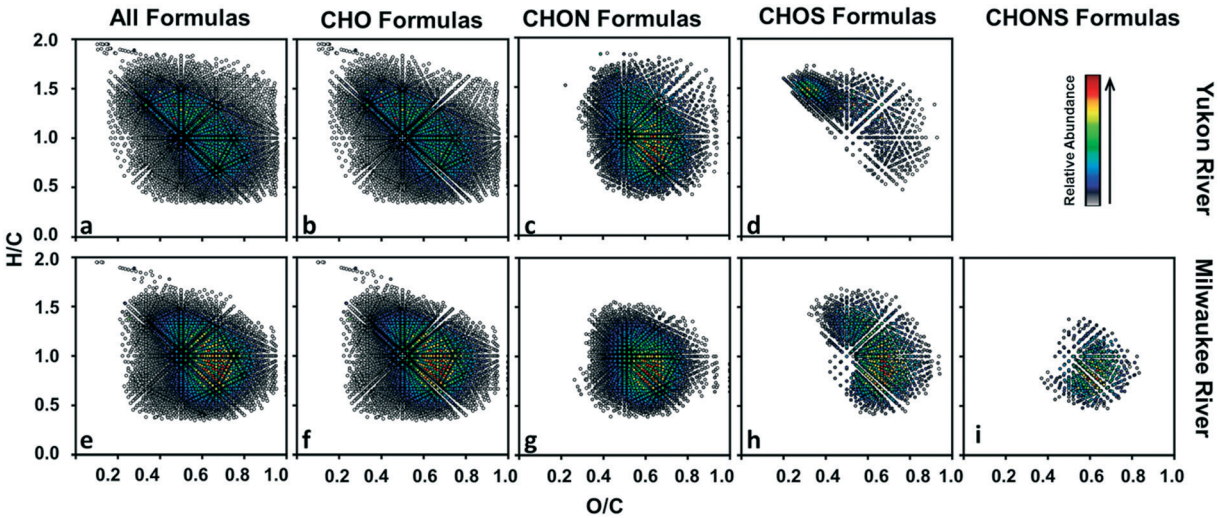

Fig. 1 van Krevelen diagrams of Yukon River (a–d) and Milwaukee River (e–i) NOM by (—) ESI 21 T FT-ICRMS: (a and e) all formulas, (b and f) CHO, (c and g) CHON, (d and h) CHOS, and (i) CHONS. NOM concentration was 5 mg L^{-1}.

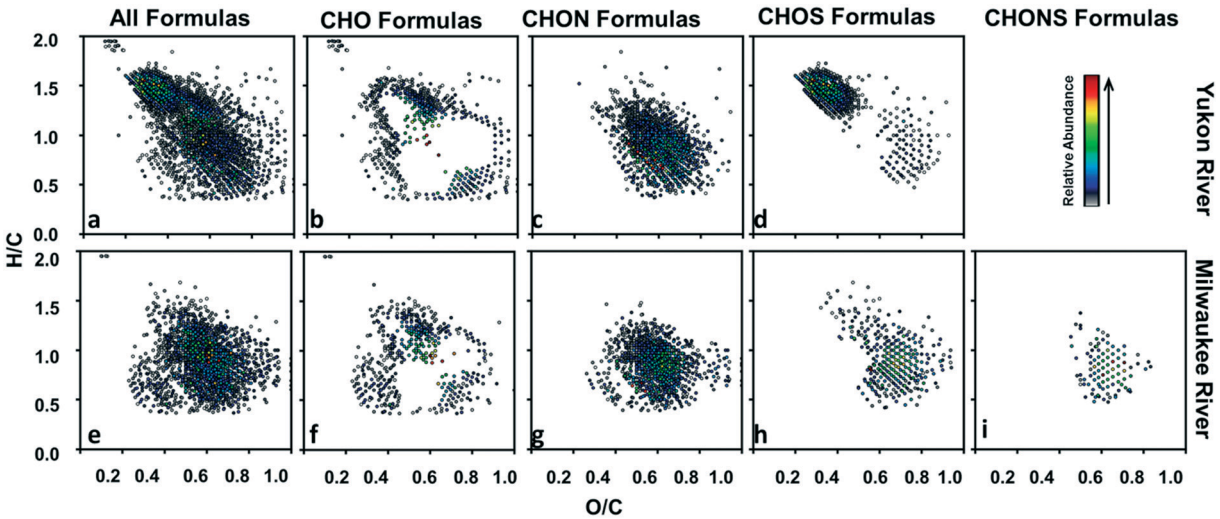

Fig. 2 van Krevelen diagrams of unique formulas to AgNM-NOM corona in Yukon River (a–d) and Milwaukee River (e–i) NOM by (—) ESI 21 T FT-ICRMS: (a and e) all formulas, (b and f) CHO, (c and g) CHON, (d and h) CHOS, and (i) CHONS. NOM concentration was 5 mg L^{-1}.

2.3% phenolic compounds. In the MRNOM, the majority of CHOS compounds were HUPC (80.5% RA), and phenolic (14.5% RA) with ~3% aliphatic and ~1% CPA.

AgNM-NOM corona is rich with HUPC (*ca.* 69–71% RA) and phenolic compounds (*ca.* 19–20% RA) for AgNM-NOM corona formed from the YRNOM and MRNOM (Fig. 3c and d and Table S3†). Condensed polycylic aromatics were slightly enriched, increasing from 4.1% RA in YRNOM to 5.7% RA in AgNM-NOM corona formed from the YRNOM and from 3.8% RA in the MRNOM to 9.1% RA in the AgNM-NOM corona formed from the MRNOM. Aliphatic formulas were <1% in AgNM-NOM corona formed from the MRNOM. This is in agreement with the limited adsorption of aliphatic formulas on the surface of other types of NMs *e.g.*, aluminum oxide,[43] and iron oxides.[57] However, aliphatic compound represented 11.3% RA in the AgNM-NOM corona formed from the YRNOM. This enrichment of aliphatic compounds is dominated by CHOS aliphatics (represent 28.6% RA of all CHOS forming AgNM-NOM corona), suggesting an important role of sulfur in the selective adsorption of these aliphatic compounds. Most likely sulfur occurs as sulfide in these compounds and AgNMs have higher affinity for S-containing ligands as discussed above. This suggests that aliphatic compounds have a negligible contribution to AgNM-NOM corona, except when aliphatic compounds have a chemical affinity to the NM surface. This is in good agreement with previous studies, where Lv *et al.* demonstrated selective adsorption of aromatic and the polyphenols to iron oxides, while aliphatic compounds were preferentially retained in the aqueous phase (*i.e.*, did not sorb on the surface of iron oxide NMs).[86] Galindo and Del Nero (2014) demonstrated fractionation of SRFA by alumina surfaces, and reported major

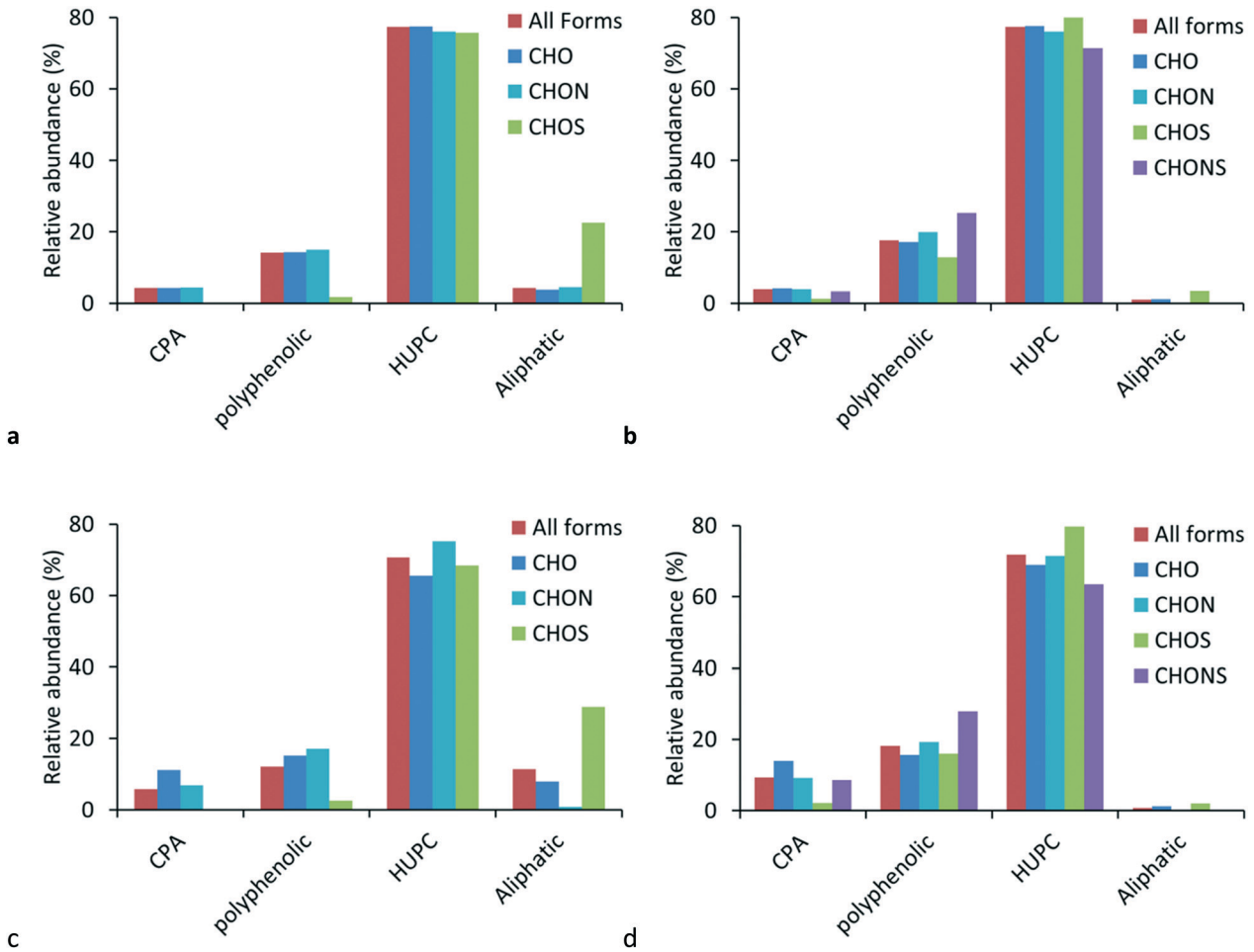

Fig. 3 Distribution of descriptive compound classes in each class of heteroatom class of compounds (a) YR-NOM, (b) MR-NOM, (c) AgNM-YRNOM-corona, and (d) AgNM-MRNOM-corona. CPA: Condensed polycyclic aromatics; HUPC: highly unsaturated and polyphenolic compounds.

removal of highly oxidized aromatic compounds and multiple oxygenated functionalities, unsaturated polycyclic aromatic compounds with fewer oxidized groups, and aliphatic compounds characterized by relatively high O/C values. It was suggested that adsorption of these compounds was due mainly to the interaction of their oxygenated functionalities with particle surfaces.[43]

3.3. Effect of NOM molecular properties on AgNM-NOM corona

The relative abundance (RA) distribution of molecular descriptors (MW, and DBE) was constructed and presented in Fig. 4. The relative abundance average molecular descriptors were calculated and summarized in Table 1 for each sample and subsequent heteroatom class. Slight differences (<10%) in the average H/C, O/C and AI_{mod} values were observed in YRNOM, MRNOM and their corresponding AgNM-NOM corona (Table 1). However, higher differences (>10%) were observed in MW and DBE values as discussed below.

Molecular weight. The broadband negative-ion ESI FT-ICR-MS mass spectra for each class of compounds in the original YRNOM (Fig. S1†) and MRNOM (Fig. S2†) and those of the corresponding AgNM-NOM corona (Fig. S3 and S4†) indicate selective adsorption of NOM formulas with higher molecular mass for each class of compounds. This is further illustrated in the shift in the MW of AgNM-NOM corona to higher values compared to those in the original NOM (Fig. 4a and c). This is in line with previous studies demonstrating the selective adsorption of higher molecular weight compounds on NMs or mineral surfaces.[86–89] For instance, Galindo demonstrated the selective adsorption of fulvic acid formulas with m/z values ranging from 120 to 980, with almost all fulvic acid formulas with $m/z \geq 775$ selectively sorbed on the surface of aluminum oxide.[43] However, few studies investigated the changes in molecular weight distribution based on heteroatom classes of compounds. The molecular weight distribution of the different heteroatom based compound classes in AgNM-NOM corona follow the order of CHO > CHON > CHOS > CHONS (Fig. S6† and Table 1). This trend in MW suggests that molecular size plays a more important role in the adsorption of CHO compounds compared to CHON and CHOS compounds, likely due to the selective adsorption of compounds with high oxygen content (see discussion below).

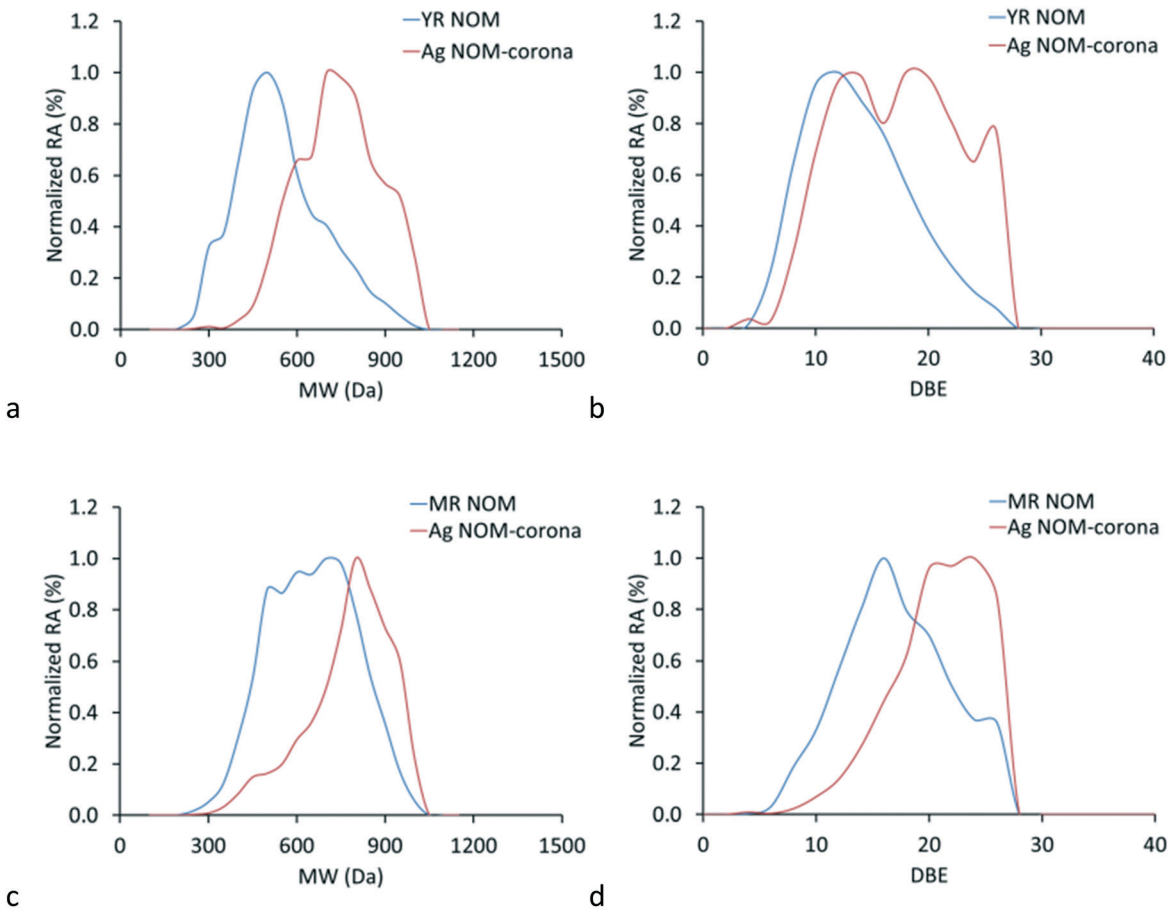

Fig. 4 Distribution of MW and DBE of molecular formulas in (a and b) Yukon River natural organic matter (YRNOM) and the corresponding NOM-corona, and (c and d) Milwaukee River natural organic matter (MRNOM) and the corresponding NOM-corona.

This could also be attributed to the differences in the mechanisms of adsorption of these different compounds. To the best of our knowledge, this is the first study to reveal the detailed selective adsorption of different molecular weight formulas for different compound classes of NOMs.

Saturation level (DBE). The distribution of DBE shows a shift toward higher DBE values for compounds forming AgNM-NOM corona compared to those in the original NOMs (Fig. 4b and d and S7,† Table 1) indicating that molecules forming AgNM-NOM corona are highly unsaturated, and/or aromatic. With increasing DBE, the degree of unsaturation and potentially aromaticity increases because higher DBE values result from addition of double bond or an aromatic ring. Molecules forming AgNM-NOM corona have a higher DBE compared to the original NOM as carbon saturation decreases and unsaturation present in functional group increases due to selective adsorption of highly oxygenated formulas on AgNM surfaces (see discussion below). Aromaticity (AI_{mod}) of NOM and AgNM-NOM corona did not change significantly.

The DBE distribution of the different heteroatom classes in AgNM-NOM corona followed the order CHO ≈ CHON > CHONS > CHOS (Fig. S7†). The distribution and average DBE of CHOS compounds in AgNM-NOM corona formed by NOM adsorption from the YRNOM increased slightly (*e.g.*, from 9.7 to 10.9, Table 1), whereas the DBE for CHOS sorbed from the MRNOM increased from 13. 6 to 17.3, possibly due to different adsorption mechanisms. Future studies are needed to investigate the effect of S-containing compounds/components in NOMs on the molecular make-up of AgNM-NOM corona using well-characterized NOM isolates with different sulfur contents and speciation.[76]

Oxygen content. Most of the compounds forming AgNM-NOM corona are highly oxygenated compounds and have high DBE values (Fig. 4b and d), suggesting that oxygen atom content and the unsaturation level of the compounds are important parameters governing their adsorption behavior. Fig. 5 depicts the number of oxygen atoms *versus* the DBE values in the molecular formulas of the original NOM and AgNM-NOM corona, and demonstrates that formulas forming AgNM-NOM corona are characterized by high DBE and high oxygen content.

Fig. S8† shows the number of oxygen atoms in each formula for the CHO, CHON, and CHOS formulas, which demonstrates that AgNM-NOM corona is rich with the highly oxygenated formulas for each class of compounds. In the YRNOM, only formulas with the highest number of oxygen (25, 20, 18, and 16 for CHON1, CHON2, CHON3, and CHOS

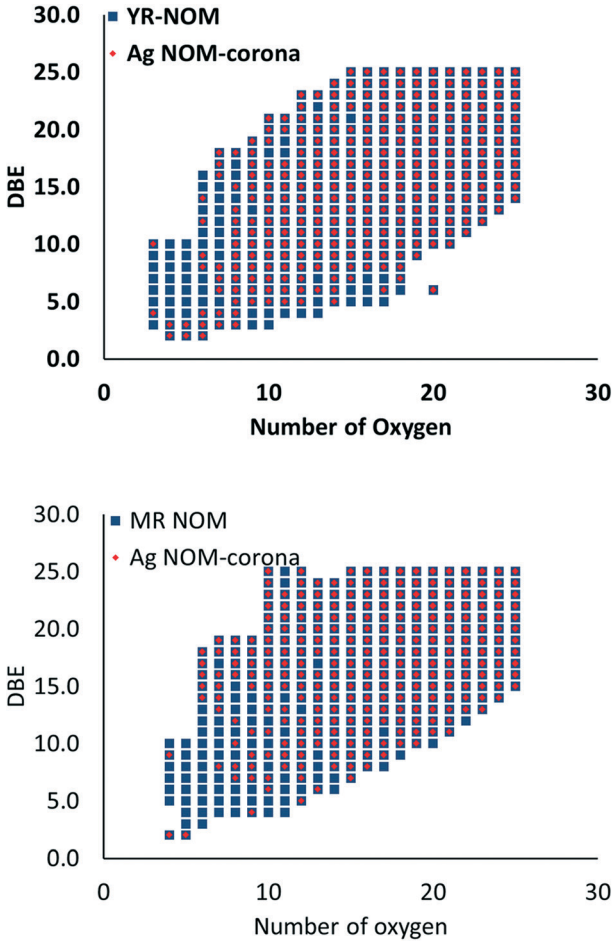

Fig. 5 Plot of DBE *versus* the number of oxygen atoms in the original NOM and Ag NOM-corona.

formulas) were fully removed from solution (*e.g.*, number of formulas in NOM and AgNM-NOM corona are equal), whereas in the MRNOM, formulas with the two highest number of oxygen (23–24, 21–22, 20–21 and 20–21 for CHON, CHON1, CHON2, CHON3 and CHOS) were totally removed on the surface of AgNMs. For CHO formulas, although the number of formulas in AgNM-NOM corona increased with the increased number of oxygen atoms in the formula, none of the formulas were completely removed from solution to AgNM surfaces (*e.g.*, number of CHO formulas in AgNM-NOM corona was always lower than number of CHO formulas in the corresponding NOM).

These observations point to the importance of oxygen (*e.g.*, oxygenated functional groups) in the binding of NOM formulas to the surface of AgNMs, presumably carboxyl group-Ag bond, *via* ligand-exchange reaction. This is in good agreement with previous studies, where oxygen-containing Suwannee River fulvic acid-corona of approximately 1.3 nm was observed around AgNMs using STEM-EELS.[56] Additionally, several studies have demonstrated the importance of oxygenated functional groups in the binding of organic ligands to Ag surfaces,[90] and to soil, minerals, and NMs.[38,42,43,86] Although, carboxylic functional groups have very low affinity to AgNMs, the affinity of organic ligand to AgNMs increase with the increase in number of carboxylates.[77]

4. Conclusions

NOM plays a pivotal role in determining NM environmental behavior such as aggregation, dissolution, uptake, and toxicity. Previous studies have focused on effects of NOM on NM aggregation, dissolution, uptake, and toxicity. Some studies focused on selective adsorption of NOM on the surface of NMs using bulk analysis techniques. However, very few studies have focused on molecular level characterization of NOM-corona. Using ESI-FT-ICR-MS, our results indicate that NOM-corona composition is a function of NOM chemical composition. Specifically, AgNM-NOM corona is rich with N- and S-containing formulas and compounds with HMW, high unsaturation, and containing high number of oxygenated groups. An exception to this is the adsorption of CHOS compounds on AgNMs in the YRNOM treatment which are characterized by low molecular weight and low unsaturation, likely resulting from selective adsorption *via* chemical complexation (Ag–S). On the other hand, NOM compounds with low molecular weight and low unsaturation or compounds containing few oxygenated groups (mainly alcohols and ethers) are preferentially maintained in solution. Similar molecular fractionation has also been observed for riverine NOM on the surface of iron oxides and for FA and HA on the surface of aluminum oxides. Therefore, the formation of NOM-corona determines to a great extent NM and NOM environmental behaviors. Future studies are needed to elucidate the interrelationship between the properties of NOM-corona and the environmental fate and behavior of NMs and NOM in aquatic environments.

Conflicts of interest

There are no conflicts to declare.

Acknowledgements

We acknowledge funding from the National Science Foundation (NSF#1738340). We thank Hui Lin for his assistance in the fluorescence characterization of NOM samples and Dr. David C Podgorski for his assistance with FT-ICR-MS analysis. All FT-ICR-MS analyses were performed at the National High Magnetic Field Laboratory, which is supported by the National Science Foundation Division of Material Research through DMR-1157490, Florida State University, and the State of Florida.

Notes and references

1 M. Filella, Colloidal properties of submicron particles in natural waters, in *Environmental colloids and particles: behaviour, structure and characterisation*, ed. K. Wilkinson and J. R. Lead, John Wiley and Sons, New York, 2007, pp. 18–93.

2 A. Nebbioso and A. Piccolo, Molecular characterization of dissolved organic matter (DOM): a critical review, *Anal. Bioanal. Chem.*, 2013, **405**(1), 109–124.

3 E. Tipping, *Cation binding by humic substances*, Cambridge University Press, Cambridge, 2002.

4 M. Rebhun, F. De Smedt and J. Rwetabula, Dissolved humic substances for remediation of sites contaminated by organic pollutants. Binding-desorption model predictions, *Water Res.*, 1996, **30**(9), 2027–2038.

5 C. T. Gibson, I. J. Turner, C. J. Roberts and J. R. Lead, Quantifying the dimensions of nanoscale organic surface layers in natural waters, *Environ. Sci. Technol.*, 2007, **41**(4), 1339–1344.

6 P. Reiller, B. Amekraz and C. Moulin, Sorption of Aldrich Humic Acid onto Hematite: Insights into Fractionation Phenomena by Electrospray Ionization with Quadrupole Time-of-Flight Mass Spectrometry, *Environ. Sci. Technol.*, 2006, **40**(7), 2235–2241.

7 M. Meier, K. Namjesnik-Dejanovic, P. A. Maurice, Y. P. Chin and G. R. Aiken, Fractionation of aquatic natural organic matter upon sorption to goethite and kaolinite, *Chem. Geol.*, 1999, **157**(3–4), 275–284.

8 I. Lynch, K. A. Dawson, J. R. Lead and E. Valsami-Jones, Macromolecular coronas and their importance in nanotoxicology and nanoecotoxicology, in *Nanoscience and the Environment*, ed. J. R. Lead and E. Valsami-Jones, 2014.

9 F. Mohd Omar, H. Abdul Aziz and S. Stoll, Aggregation and disaggregation of ZnO nanoparticles: Influence of pH and adsorption of Suwannee River humic acid, *Sci. Total Environ.*, 2014, **468**, 195–201.

10 S. Ghosh, W. Jiang, J. D. McClements and B. Xing, Colloidal Stability of Magnetic Iron Oxide Nanoparticles: Influence of Natural Organic Matter and Synthetic Polyelectrolytes, *Langmuir*, 2011, **27**(13), 8036–8043.

11 F. Loosli, P. Le Coustumer and S. Stoll, TiO2 nanoparticles aggregation and disaggregation in presence of alginate and Suwannee River humic acids. pH and concentration effects on nanoparticle stability, *Water Res.*, 2013, **47**(16), 6052–6063.

12 I. L. Gunsolus, M. P. Mousavi, K. Hussein, P. Bühlmann and C. L. Haynes, Effects of humic and fulvic acids on silver nanoparticle stability, dissolution, and toxicity, *Environ. Sci. Technol.*, 2015, **49**(13), 8078–8086.

13 Z. Linlin and K. Tanaka, Dissolution of silver nanoparticles in presence of natural organic matter, *Adv. Mater. Lett.*, 2014, **5**(1), 6–8.

14 M. Baalousha, K. P. Arkill, I. Romer, R. E. Palmer and J. R. Lead, Transformations of citrate and Tween coated silver nanoparticles reacted with Na2S, *Sci. Total Environ.*, 2015, **502**(0), 344–353.

15 Y. Zhang, J. Xia, Y. Liu, L. Qiang and L. Zhu, Impacts of Morphology, Natural Organic Matter, Cations, and Ionic Strength on Sulfidation of Silver Nanowires, *Environ. Sci. Technol.*, 2016, **50**(24), 13283–13290.

16 S. M. Kteeba, H. I. El-Adawi, O. A. El-Rayis, A. E. El-Ghobashy, J. L. Schuld, K. R. Svoboda and L. D. Guo, Zinc oxide nanoparticle toxicity in embryonic zebrafish: Mitigation with different natural organic matter, *Environ. Pollut.*, 2017, **230**, 1125–1141, DOI: 10.1016/j.envpol.2017.07.042.

17 B. Gu, J. Schmitt, Z. Chen, L. Liang and J. F. McCarthy, Adsorption and desorption of natural organic matter on iron oxide: mechanisms and models, *Environ. Sci. Pollut. Res.*, 1994, **28**, 38–46.

18 S. M. Louie, E. R. Spielman-Sun, M. J. Small, R. D. Tilton and G. V. Lowry, Correlation of the Physicochemical Properties of Natural Organic Matter Samples from Different Sources to Their Effects on Gold Nanoparticle Aggregation in Monovalent Electrolyte, *Environ. Sci. Technol.*, 2015, **49**(4), 2188–2198.

19 S. M. Louie, R. D. Tilton and G. V. Lowry, Effects of Molecular Weight Distribution and Chemical Properties of Natural Organic Matter on Gold Nanoparticle Aggregation, *Environ. Sci. Technol.*, 2013, **47**(9), 4245–4254.

20 J. A. Nason, S. A. McDowell and T. W. Callahan, Effects of natural organic matter type and concentration on the aggregation of citrate-stabilized gold nanoparticles, *J. Environ. Monit.*, 2012, **14**(7), 1885–1892.

21 M. H. Shen, Y. G. Yin, A. Booth and J. F. Liu, Effects of molecular weight-dependent physicochemical heterogeneity of natural organic matter on the aggregation of fullerene nanoparticles in mono- and di-valent electrolyte solutions, *Water Res.*, 2015, **71**, 11–20.

22 A. Deonarine, B. L. T. Lau, G. R. Aiken, J. N. Ryan and H. Hsu-Kim, Effects of Humic Substances on Precipitation and Aggregation of Zinc Sulfide Nanoparticles, *Environ. Sci. Technol.*, 2011, **45**(8), 3217–3223.

23 X. Yang, C. Jiang, H. Hsu-Kim, A. R. Badireddy, M. Dykstra, M. Wiesner, D. E. Hinton and J. N. Meyer, Silver Nanoparticle Behavior, Uptake, and Toxicity in Caenorhabditis elegans: Effects of Natural Organic Matter, *Environ. Sci. Technol.*, 2014, **48**(6), 3486–3495.

24 S. W. Bian, I. A. Mudunkotuwa, T. Rupasinghe and V. H. Grassian, Aggregation and Dissolution of 4 nm ZnO Nanoparticles in Aqueous Environments: Influence of pH, Ionic Strength, Size, and Adsorption of Humic Acid, *Langmuir*, 2011, **27**(10), 6059–6068.

25 L. F. Wang, N. Habibul, D. Q. He, W. W. Li, X. Zhang, H. Jiang and H. Q. Yu, Copper release from copper nanoparticles in the presence of natural organic matter, *Water Res.*, 2015, **68**, 12–23.

26 T. P. Dasari and H. M. Hwang, The effect of humic acids on the cytotoxicity of silver nanoparticles to a natural aquatic bacterial assemblage, *Sci. Total Environ.*, 2010, **408**(23), 5817–5823.

27 J. Fabrega, S. R. Fawcett, J. C. Renshaw and J. R. Lead, Silver Nanoparticle Impact on Bacterial Growth: Effect of pH, Concentration, and Organic Matter, *Environ. Sci. Technol.*, 2009, **43**(19), 7285–7290.

28 S. M. Wirth, G. V. Lowry and R. D. Tilton, Natural Organic Matter Alters Biofilm Tolerance to Silver Nanoparticles and Dissolved Silver, *Environ. Sci. Technol.*, 2012, **46**(22), 12687–12696.

29 X. Liu, X. Jin, B. Cao and C. Y. Tang, Bactericidal activity of silver nanoparticles in environmentally relevant freshwater matrices: Influences of organic matter and chelating agent, *J. Environ. Chem. Eng.*, 2014, **2**(1), 525–531.

30 A. Ücer, A. Uyanik and S. P. Aygün, Adsorption of Cu(II), Cd(II), Zn(II), Mn(II) and Fe(III) ions by tannic acid immobilised activated carbon, *Sep. Purif. Technol.*, 2006, **47**(3), 113–118.

31 K. Afshinnia, I. Gibson, R. Merrifield and M. Baalousha, The concentration-dependent aggregation of Ag NPs induced by cystine, *Sci. Total Environ.*, 2016, **557–558**, 395–403.

32 A. P. Gondikas, A. Morris, B. C. Reinsch, S. M. Marinakos, G. V. Lowry and H. Hsu-Kim, Cysteine-induced modifications of zero-valent silver nanomaterials: Implications for particle surface chemistry, aggregation, dissolution, and silver speciation, *Environ. Sci. Technol.*, 2012, **46**(13), 7037–7045.

33 S. P. Yang, O. Bar-Ilan, R. E. Peterson, W. Heideman, R. J. Hamers and J. A. Pedersen, Influence of Humic Acid on Titanium Dioxide Nanoparticle Toxicity to Developing Zebrafish, *Environ. Sci. Technol.*, 2013, **47**(9), 4718–4725.

34 F. Claret, T. Schäfer, J. Brevet and P. E. Reiller, Fractionation of Suwannee River Fulvic Acid and Aldrich Humic Acid on α-Al2O3: Spectroscopic Evidence, *Environ. Sci. Technol.*, 2008, **42**(23), 8809–8815.

35 S. GHOSH, Z. Y. WANG, S. Kang, P. C. BHOWMIK and B. S. Xing, Sorption and Fractionation of a Peat Derived Humic Acid by Kaolinite, Montmorillonite, and Goethite, *Pedosphere*, 2009, **19**(1), 21–30.

36 K. Kaiser, Sorption of natural organic matter fractions to goethite (α-FeOOH): effect of chemical composition as revealed by liquid-state 13C NMR and wet-chemical analysis, *Org. Geochem.*, 2003, **34**(11), 1569–1579.

37 J. Hur and M. A. Schlautman, Effects of pH and phosphate on the adsorptive fractionation of purified Aldrich humic acid on kaolinite and hematite, *J. Colloid Interface Sci.*, 2004, **277**(2), 264–270.

38 S. Avneri-Katz, R. B. Young, A. M. McKenna, H. Chen, Y. E. Corilo, T. Polubesova, T. Borch and B. Chefetz, Adsorptive fractionation of dissolved organic matter (DOM) by mineral soil: Macroscale approach and molecular insight, *Org. Geochem.*, 2017, **103**, 113–124.

39 L. Guo and P. H. Santschi, Ultrafiltration and its applications to sampling and characterization of aquatic colloids, in *Environmental colloids and particles: behaviour, separation and characterization*, ed. K. J. Wilkinson and J. R. Lead, John Wiley & Sons Ltd, Chichester, 2007, pp. 159–222.

40 N. Hertkorn, M. Frommberger, M. Witt, B. P. Koch, P. Schmitt-Kopplin and E. M. Perdue, Natural Organic Matter and the Event Horizon of Mass Spectrometry, *Anal. Chem.*, 2008, **80**(23), 8908–8919.

41 J. D'Andrilli, T. Dittmar, B. P. Koch, J. M. Purcell, A. G. Marshall and W. T. Cooper, Comprehensive characterization of marine dissolved organic matter by Fourier transform ion cyclotron resonance mass spectrometry with electrospray and atmospheric pressure photoionization, *Rapid Commun. Mass Spectrom.*, 2010, **24**(5), 643–650.

42 C. Galindo and M. Del Nero, Chemical fractionation of a terrestrial humic acid upon sorption on alumina by high resolution mass spectrometry, *RSC Adv.*, 2015, **5**(89), 73058–73067.

43 C. Galindo and M. Del Nero, Molecular Level Description of the Sorptive Fractionation of a Fulvic Acid on Aluminum Oxide Using Electrospray Ionization Fourier Transform Mass Spectrometry, *Environ. Sci. Technol.*, 2014, **48**(13), 7401–7408.

44 L. Guo and R. W. Macdonald, Source and transport of terrigenous organic matter in the upper Yukon River: Evidence from isotope (δ13C, Δ14C, and δ15N) composition of dissolved, colloidal, and particulate phases, *Global Biogeochem. Cycles*, 2006, **20**(2), BG2011.

45 J. L. Weishaar, G. R. Aiken, B. A. Bergamaschi, M. S. Fram, R. Fujii and K. Mopper, Evaluation of Specific Ultraviolet Absorbance as an Indicator of the Chemical Composition and Reactivity of Dissolved Organic Carbon, *Environ. Sci. Technol.*, 2003, **37**(20), 4702–4708.

46 C. L. Hendrickson, J. P. Quinn, N. K. Kaiser, D. F. Smith, G. T. Blakney, T. Chen, A. G. Marshall, C. R. Weisbrod and S. C. Beu, 21 Tesla Fourier Transform Ion Cyclotron Resonance Mass Spectrometer: A National Resource for Ultrahigh Resolution Mass Analysis, *J. Am. Soc. Mass Spectrom.*, 2015, **26**(9), 1626–1632.

47 T. Dittmar, B. Koch, N. Hertkorn and G. Kattner, A simple and efficient method for the solid-phase extraction of dissolved organic matter (SPE-DOM) from seawater, *Limnol. Oceanogr.: Methods*, 2008, **6**(6), 230–235.

48 M. M. Tfaily, S. Hodgkins, D. C. Podgorski, J. P. Chanton and W. T. Cooper, Comparison of dialysis and solid-phase extraction for isolation and concentration of dissolved organic matter prior to Fourier transform ion cyclotron resonance mass spectrometry, *Anal. Bioanal. Chem.*, 2012, **404**(2), 447–457.

49 S. D. H. Shi, J. J. Drader, M. A. Freitas, C. L. Hendrickson and A. G. Marshall, Comparison and interconversion of the two most common frequency-to-mass calibration functions for Fourier transform ion cyclotron resonance mass spectrometry, *Int. J. Mass Spectrom.*, 2000, **195–196**, 591–598.

50 J. J. Savory, N. K. Kaiser, A. M. McKenna, F. Xian, G. T. Blakney, R. P. Rodgers, C. L. Hendrickson and A. G. Marshall, Parts-Per-Billion Fourier Transform Ion Cyclotron Resonance Mass Measurement Accuracy with a "Walking" Calibration Equation, *Anal. Chem.*, 2011, **83**(5), 1732–1736.

51 B. P. Koch and T. Dittmar, From mass to structure: an aromaticity index for high-resolution mass data of natural organic matter, *Rapid Commun. Mass Spectrom.*, 2006, **20**(5), 926–932.

52 A. S. Willoughby, A. S. Wozniak and P. G. HATCHER, A molecular-level approach for characterizing water-insoluble components of ambient organic aerosol particulates using ultrahigh-resolution mass spectrometry, *Atmos. Chem. Phys.*, 2014, **14**(18), 10299–10314.

53 Y. Zhao, A. G. Hallar and L. R. Mazzoleni, Atmospheric organic matter in clouds: exact masses and molecular formula identification using ultrahigh-resolution FT-ICR

mass spectrometry, *Atmos. Chem. Phys.*, 2013, **13**(24), 12343–12362.
54 M. Baalousha, A. Manciulea, S. Cumberland, K. Kendall and J. R. Lead, Aggregation and surface properties of iron oxide nanoparticles, influence of pH and natural organic matter, *Environ. Toxicol. Chem.*, 2008, **27**(9), 1875–1882.
55 M. Baalousha, Aggregation and disaggregation of iron oxide nanoparticles: Influence of particle concentration, pH and natural organic matter, *Sci. Total Environ.*, 2009, **407**(6), 2093–2101.
56 I. Römer, Z. W. Wang, R. C. Merrifield, R. E. Palmer and J. Lead, High Resolution STEM-EELS Study of Silver Nanoparticles Exposed to Light and Humic Substances, *Environ. Sci. Technol.*, 2016, **50**(5), 2183–2190.
57 T. Riedel, H. Biester and T. Dittmar, Molecular Fractionation of Dissolved Organic Matter with Metal Salts, *Environ. Sci. Technol.*, 2012, **46**(8), 4419–4426.
58 S. Kim, R. W. Kramer and P. G. HATCHER, Graphical Method for Analysis of Ultrahigh-Resolution Broadband Mass Spectra of Natural Organic Matter, the Van Krevelen Diagram, *Anal. Chem.*, 2003, **75**(20), 5336–5344.
59 A. Piccolo, The supramolecular structure of humic substances, *Soil Sci.*, 2001, **166**, 810–832.
60 A. M. Graham, G. R. Aiken and C. C. Gilmour, Effect of Dissolved Organic Matter Source and Character on Microbial Hg Methylation in Hg-S-DOM Solutions, *Environ. Sci. Technol.*, 2013, **47**(11), 5746–5754.
61 A. Manceau and K. L. Nagy, Quantitative analysis of sulfur functional groups in natural organic matter by XANES spectroscopy, *Geochim. Cosmochim. Acta*, 2012, **99**(Supplement C), 206–223.
62 J. Xu, J. Wu and Y. He, *Functions of natural organic matter in changing environment*, Springer Science & Business Media, 2013.
63 G. R. Aiken, H. Hsu-Kim and J. N. Ryan, Influence of Dissolved Organic Matter on the Environmental Fate of Metals, Nanoparticles, and Colloids, *Environ. Sci. Technol.*, 2011, **45**(8), 3196–3201.
64 M. P. Mousavi, I. L. Gunsolus, C. E. Pérez De Jesús, M. Lancaster, K. Hussein, C. L. Haynes and P. Bühlmann, Dynamic silver speciation as studied with fluorous-phase ion-selective electrodes: Effect of natural organic matter on the toxicity and speciation of silver, *Sci. Total Environ.*, 2015, **537**, 453–461.
65 C. N. Glover, S. K. Sharma and C. M. Wood, Heterogeneity in physicochemical properties explains differences in silver toxicity amelioration by natural organic matter to Daphnia magna, *Environ. Toxicol. Chem.*, 2005, **24**(11), 2941–2947.
66 F. J. Sikora and F. J. Stevenson, Silver complexation by humic substances: Conditional stability constants and nature of reactive sites, *Geoderma*, 1988, **42**(3–4), 353–363.
67 P. L. Cloke, The geologic role of polysulfides–Part II: The solubility of acanthite and covellite in sodium polysulfide solutions, *Geochim. Cosmochim. Acta*, 1963, **27**(12), 1299–1319.
68 M. M. Alshammari, *Determination of Silver Binding to Natural Organic Matter Using Ion Selective Electrode*, 2017.
69 A. S. Douglas, *Fundamentals of analytical chemistry*, Grupo Editorial Norma, 2004.
70 D. C. Harris, *Quantitative chemical analysis*, Macmillan, 2010.
71 G. L. Bovenkamp, U. Zanzen, K. S. Krishna, J. Hormes and A. Prange, X-ray absorption near-edge structure (XANES) spectroscopy study of the interaction of silver ions with Staphylococcus aureus, Listeria monocytogenes, and Escherichia coli, *Appl. Environ. Microbiol.*, 2013, **79**(20), 6385–6390.
72 M. Haitzer, G. R. Aiken and J. N. Ryan, Binding of Mercury(II) to Aquatic Humic Substances: Influence of pH and Source of Humic Substances, *Environ. Sci. Technol.*, 2003, **37**(11), 2436–2441.
73 A. Vairavamurthy, Using X-ray absorption to probe sulfur oxidation states in complex molecules, *Spectrochim. Acta, Part A*, 1998, **54**(12), 2009–2017.
74 S. J. Yoon, L. M. Diener, P. R. Bloom, E. A. Nater and W. F. Bleam, X-ray absorption studies of CH3Hg+−binding sites in humic substances, *Geochim. Cosmochim. Acta*, 2005, **69**(5), 1111–1121.
75 J. S. Waples, K. L. Nagy, G. R. Aiken and J. N. Ryan, Dissolution of cinnabar (HgS) in the presence of natural organic matter, *Geochim. Cosmochim. Acta*, 2005, **69**(6), 1575–1588.
76 B. A. Poulin, J. N. Ryan, K. L. Nagy, A. Stubbins, T. Dittmar, W. Orem, D. P. Krabbenhoft and G. R. Aiken, Spatial Dependence of Reduced Sulfur in Everglades Dissolved Organic Matter Controlled by Sulfate Enrichment, *Environ. Sci. Technol.*, 2017, **51**(7), 3630–3639.
77 R. A. Bell and J. R. Kramer, Structural chemistry and geochemistry of silver-sulfur compounds: Critical review, *Environ. Toxicol. Chem.*, 1999, **18**(1), 9–22.
78 I. G. Dance, The structural chemistry of metal thiolate complexes, *Polyhedron*, 1986, **5**(5), 1037–1104.
79 S. Krzewska and H. Podsiadly, Complexes of Ag(I) with ligands containing sulphur donor atoms, *Polyhedron*, 1986, **5**(4), 937–944.
80 H. R. Schulten and M. Schnitzer, The chemistry of soil organic nitrogen: a review, *Biol. Fertil. Soils*, 1997, **26**(1), 1–15.
81 K. A. Thorn and L. G. Cox, N-15 NMR spectra of naturally abundant nitrogen in soil and aquatic natural organic matter samples of the International Humic Substances Society, *Org. Geochem.*, 2009, **40**(4), 484–499.
82 J. Lehmann, D. Solomon, J. Brandes, H. Fleckenstein, C. Jacobson and J. Thieme, Synchrotron-Based Near-Edge X-Ray Spectroscopy of Natural Organic Matter in Soils and Sediments, in *Biophysico-Chemical Processes Involving Natural Nonliving Organic Matter in Environmental Systems*, John Wiley & Sons, Inc., 2009, pp. 729–781.
83 A. Vairavamurthy and S. Wang, Organic Nitrogen in Geomacromolecules: Insights on Speciation and Transformation with K-edge XANES Spectroscopy, *Environ. Sci. Technol.*, 2002, **36**(14), 3050–3056.
84 S. Basu, S. Jana, S. Pande and T. Pal, Interaction of DNA bases with silver nanoparticles: Assembly quantified through SPRS and SERS, *J. Colloid Interface Sci.*, 2008, **321**(2), 288–293.

85 S. Mukherjee and M. Mukherjee, Nitrogen-mediated interaction in polyacrylamide-silver nanocomposites, *J. Phys.: Condens. Matter*, 2006, **18**(49), 11233.

86 J. Lv, S. Zhang, S. Wang, L. Luo, D. Cao and P. Christie, Molecular-Scale Investigation with ESI-FT-ICR-MS on Fractionation of Dissolved Organic Matter Induced by Adsorption on Iron Oxyhydroxides, *Environ. Sci. Technol.*, 2016, **50**(5), 2328–2336.

87 Q. Zhou, P. A. Maurice and S. E. Cabaniss, Size fractionation upon adsorption of fulvic acid on goethite: equilibrium and kinetic studies, *Geochim. Cosmochim. Acta*, 2001, **65**(5), 803–812.

88 J. A. Davis and R. Gloor, Adsorption of dissolved organics in lake water by aluminum oxide. Effect of molecular weight, *Environ. Sci. Technol.*, 1981, **15**(10), 1223–1229.

89 P. Mwaanga, E. Carraway and M. Schlautman, Preferential sorption of some natural organic matter fractions to titanium dioxide nanoparticles: influence of pH and ionic strength, *Environ. Monit. Assess.*, 2014, **186**(12), 8833–8844.

90 S. S. Naz, M. R. Shah, N. U. Islam, A. Khan, S. Nazir, S. Qaisar and S. S. Alam, Synthesis and bioactivities of silver nanoparticles capped with 5-Amino-?-resorcylic acid hydrochloride dihydrate, *J. Nanobiotechnol.*, 2014, **12**(1), 34.